

# Stimulated emission in plasma-enhanced chemical vapour deposited silicon nanocrystals

L. Dal Negro<sup>a,\*</sup>, M. Cazzanelli<sup>a</sup>, N. Daldosso<sup>a</sup>, Z. Gaburro<sup>a</sup>, L. Pavesi<sup>a</sup>,  
F. Priolo<sup>b</sup>, D. Pacifici<sup>b</sup>, G. Franzò<sup>b</sup>, F. Iacona<sup>c</sup>

<sup>a</sup>INFM and Dipartimento di Fisica, Università di Trento, I-38050 Povo (Trento), Italy

<sup>b</sup>INFM and Dipartimento di Fisica, Università di Catania, I-95129 Catania, Italy

<sup>c</sup>CNR-IMM, Sezione di Catania, I-95121 Catania, Italy

## Abstract

Observation of optical gain in silicon nanocrystals (Si-nc) is critically dependent on a very delicate balance among the Si-nc gain cross-sections, the optical mode losses and confinement factors of the waveguide structures, the Si-nc concentration and the strongly competing fast non-radiative Auger processes. Here we report on optical gain measurements by variable stripe length (VSL) method on a set of silicon nanocrystals formed by thermal annealing at 1250°C of SiO<sub>x</sub> films with different silicon contents prepared by plasma-enhanced chemical vapour deposition. Time-resolved VSL has revealed fast component in the recombination dynamics under gain conditions. Fast lifetime narrowing and superlinear emission has been unambiguously observed. To explain our experimental results we propose a four levels recombination model. Within a phenomenological rate equations description including Auger processes and amplified spontaneous emission we obtained a satisfactory agreement with time-resolved experiments and explained the strong competition between stimulated emission and fast non-radiative Auger processes.

© 2002 Elsevier Science B.V. All rights reserved.

PACS: 81.07.Bc; 78.67.Bf; 78.45.+h

Keywords: Silicon nanocrystals; Optical gain; Stimulated emission; Light amplification

## 1. Introduction

Silicon is an indirect band gap material and therefore light emission is a phonon mediated process with low probability. In standard bulk silicon, competitive non-radiative recombination rates are much higher than the radiative ones and most of the excited electron–hole pairs recombine non-radiatively.

This yields very low internal quantum efficiency for silicon luminescence. In addition, fast non-radiative processes such as *Auger* or *free carrier absorption* severely prevent population inversion in bulk Si at the high pumping rates needed to achieve optical amplification [1]. In the last decade, an intense research activity has been devoted to study different approaches to make Si a better light emitter. In particular, since the discovery of very intense room temperature visible light emission in porous silicon (p-Si) by Canham at the beginning of the 1990 [2], many different approaches have been pursued which include p-Si [3,4], silicon nanocrystals (Si-nc)

\* Corresponding author. Tel.: +39-0461-881504; fax: +39-0461-881696.

E-mail address: [dalnagro@science.unitn.it](mailto:dalnagro@science.unitn.it) (L. Dal Negro).

Table 1

Principal structural and optical parameters of the samples. Total Si in Si-nc refers to the total atomic percentage of Si in silicon nanocrystals measured by X-ray absorption measurements [32].  $R_{\text{Si-nc}}$  and  $\Delta R_{\text{Si-nc}}$  are the mean value and the width of the radii distribution of the Si-nc measured by TEM,  $\lambda_{\text{max}}^{\text{PL}}$  and  $\Delta\lambda^{\text{PL}}$  the wavelength of the maximum and width of the luminescence emission band,  $I^{\text{PL}}$  the luminescence intensity in arbitrary units for a fixed low pumping power,  $n$  the refractive index of the samples measured by m-line measurements at 633 nm,  $\Gamma$  the optical confinement factor,  $\rho$  the Si-nc density in the sample estimated by X-ray measurements,  $\sigma_{\text{g}}$  the Si-nc gain cross section at 750 nm and  $\lambda_{\text{max}}^{\text{g}}$  the wavelength of the maximum gain

Sample name	Total Si in the film (at%)	Total Si in Si-nc (at%)	$R_{\text{Si-nc}}$ (nm)	$\Delta R_{\text{Si-nc}}$ (nm)	$\lambda_{\text{max}}^{\text{PL}}$ (nm)	$\Delta\lambda^{\text{PL}}$ (nm)	$I^{\text{PL}}$	$n$	$\Gamma$	$\rho$ (cm <sup>-3</sup> )	$\sigma_{\text{g}}$ (cm <sup>2</sup> )	$\lambda_{\text{max}}^{\text{g}}$ (nm)
1A	46	19	2.1	1.2	938	215	0.86	2	0.83	$4.6 \times 10^{18}$	$4.3 \times 10^{-17}$	721
3A	42	13	1.7	1.1	906	188	3.39	1.82	0.76	$6.3 \times 10^{18}$	$3.6 \times 10^{-17}$	751
5A	39	8.5	1.5	0.7	795	136	4.68	1.66	0.63	$8.33 \times 10^{18}$	—	—

produced by several different techniques [5–8] (chemical vapour deposition, ion implantation in SiO<sub>2</sub>, laser ablation, gas evaporation, sputter deposition, electrochemical dispersion) and Si/insulator multilayers [9,10]. These last two systems are much more stable than p-Si, which still remains a very fragile material not compatible with standard silicon processing. Also the electrical pumping of Si-nc has been demonstrated and, despite of the initial difficulties, silicon LEDs are now only a factor of ten out of the demanding optoelectronic market requirements [11]. The main future challenge for silicon microphotronics is the demonstration of laser action in silicon-based materials. This result would allow low cost integration of optoelectronic functions on a single silicon chip, representing one of the most outstanding technological achievements. Following the initial observation of optical gain in Si-nc prepared by ion-implantation [12], other works [13–15] have demonstrated the possibility of stimulated emission in Si-nc despite of the severe competition with fast non-radiative processes. Although a clear understanding of the microscopic gain mechanism is still under debate, it has been realized that interface radiative states associated to oxygen atoms can play a crucial rule in determining the emission properties of the Si-nc systems [16].

## 2. Silicon nanocrystal samples

We studied Si-nc samples produced by high temperature annealing of substoichiometric silicon oxide (SiO<sub>x</sub>) thin films grown by plasma-enhanced chem-

ical vapour deposition (PECVD). The structural and luminescence properties of such systems have been fully discussed in Ref. [17]. Here we focus on a set of three different samples produced with an annealing temperature at 1250°C for 1 h and with different total Si content in the deposited oxide: 46 at% (named 1A), 42 at% (named 3A) and 39 at% (named 5A). Some of their characteristics are reported in Table 1. The annealing temperature at 1250°C maximizes the PL intensity for a fixed annealing time of 1 h. The oxide layer containing Si-nc was 250 nm thick and was embedded between two 100 nm thick stoichiometric SiO<sub>2</sub> layers to form a waveguide in order to perform VSL measurements accurately. The waveguide was formed on a transparent quartz substrate. An example of the optical mode profile and of the refractive index profile is shown in Fig. 1. By such simulation the optical mode confinement factor  $\Gamma$  can be computed. The mean radii of the investigated Si-nc sample, the FWHM of the size distribution, the linear refractive indexes, the waveguide  $\Gamma$  factors, the Si-nc volume density, the measured gain cross-section and the peak gain wavelength are all summarised in Table 1.

Fig. 2 shows the luminescence and absorbance spectra of the studied Si-nc samples. The luminescence peak shifts to higher energies with decreasing the mean Si-nc radius while the line width of the luminescence bands narrows and the luminescence intensity increases as the Si-nc size decreases. The absorption of the active Si-nc layers increases at high energy as expected on the basis of the quantum confinement model. Remarkable is the big Stokes-shift between absorption edges and emission peaks. No

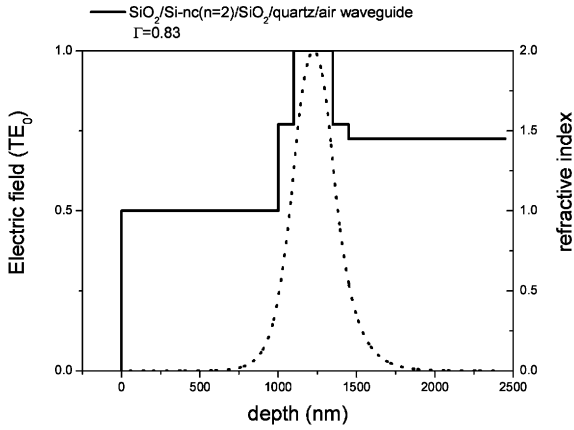


Fig. 1. Spatial mode profile of the waveguide structure for one representative Si-nc sample. Calculation has been performed by assuming a refractive index of two for the layer containing Si-nc and an effective 4 layers planar waveguide. The figure shows the modelling of the sample 1A (39 at% Si).

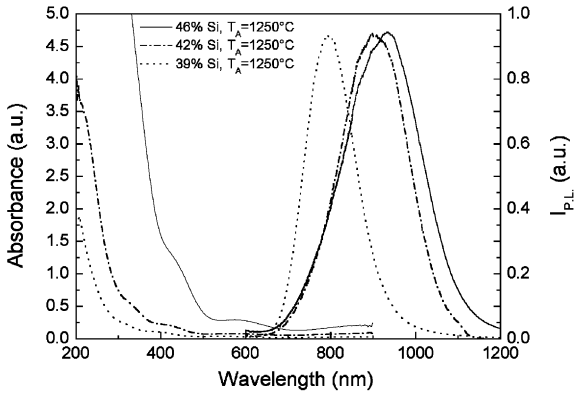


Fig. 2. Room temperature absorbance and normalized luminescence spectra of the Si-nc samples. The luminescence spectra were excited by the 488 nm Argon line at a pumping power of 5 mW and recorded by a germanium detector. Absorbance measurements were performed by a standard UV-visible double beam spectrophotometer.

appreciable absorption has been measured in the wavelength region where the luminescence maxima occur. A large debate on the origin of the luminescence is still present. Many theoretical [16,18–21] as well as experimental [5,22,23] works suggest as the origin of the luminescence the radiative recombination of an exciton trapped in an interfacial state

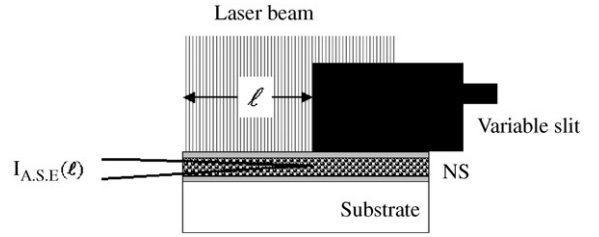


Fig. 3. Sketch of the variable stripe length configuration. The amplified spontaneous luminescence intensity  $I_{ASE}$  is collected from the edge of the sample as a function of the excitation length  $\ell$ . The laser beam is focused on a thin strip by a cylindrical lens.

formed at the Si=O bonds (silanone) present at the interface between the Si-nc and the SiO<sub>2</sub> matrix.

### 3. Variable stripe length measurements

We measured light amplification by using the variable stripe length (VSL) method [24]. In the VSL method the sample is optically excited by a laser beam in a stripe-like geometry (Fig. 3). The amplified spontaneous emission signal  $I_{ASE}$  is collected as a function of the illuminated length  $\ell$  from the edge of the sample, in a 90° configuration with respect to the excitation. As a result of stimulated emission, the spontaneous emitted light is amplified along the amplification axis of the sample (waveguide axis). Referring to a simple one-dimensional amplification model, it is possible to relate the amplified spontaneous emission intensity with the small signal modal gain coefficient  $g_{mod}$  and with the length  $\ell$  of the excited region

$$I_{ASE}(\ell) = \frac{J_{sp}(\Omega)}{g_{mod}} (e^{g_{mod}\ell} - 1), \quad (1)$$

where  $J_{sp}$  is the spontaneous emitted power corresponding to an appropriate emission solid angle  $\Omega$ .<sup>1</sup> The modal gain coefficient is related to the material gain coefficient  $g_m$  through the confinement factor  $\Gamma$  of the waveguide,  $g_{mod} = \Gamma g_m$ .

From a fit of the experimental data with Eq. (1), the net modal gain coefficient  $g'_{mod} = \Gamma g_m - \alpha$  (modal

<sup>1</sup> Considering a cylindrically shaped active medium the solid angle  $\Omega$  is the angle subtended by one face of the cylinder as seen from the centre of the other face.

gain minus the propagation losses  $\alpha$ ) can be deduced for every wavelength within the emission spectrum.

Although simple in principle, the VSL technique demands special attentions. Conceptual as well as experimental flaws can easily arise. The one-dimensional amplification model becomes meaningless at the gain-length products where gain saturation begins to set in. Once the gain saturation intensity  $I_{\text{sat}}$  is determined, the limit  $g\ell$  can be approximately estimated by using the following equation [25]:

$$g\ell \leq \ln\left(\frac{\lambda^5 I_{\text{sat}}}{\pi h c^2 \Omega \Delta\lambda}\right), \quad (2)$$

where  $\lambda$  is the emission wavelength,  $\Delta\lambda$  the emission line shape and  $\Omega$  the emission solid angle.

Assuming a gain cross-section of  $10^{-17} \text{ cm}^2$  for the Si-nc and a recombination lifetime in the  $\mu\text{s}$  range, the VSL measurement can be performed on our samples only for  $g\ell \leq 10$ . For higher  $\ell$ , the application of Eq. (1) is not justified.

A much more subtle experimental difficulty arises from the pump diffraction caused by the variable slit, as well as by the straight edge of the sample itself. This causes non-constant pump intensity on the sample surface, in contrast to the implicit assumption of the one-dimensional amplifier model. In order to overcome this diffraction problem, we measured the diffraction intensity as a function of  $\ell$ , simply by performing the VSL measurement at the laser beam wavelength. The data are compared with a Fresnel straight edge diffraction calculation [26] in Fig. 4. From this diffraction analysis, we are able to monitor the uniformity of the sample excitation during the VSL measurements simply collecting at every fixed  $\ell$  the luminescence signal and the diffracted pump laser intensity separately. From the specific example of Fig. 4, it is clear that the pumping intensity can be considered constant on the sample only in the  $\ell$  range from 0.02 to 0.06 cm, where the zero is arbitrary: this is the appropriate length interval where the one-dimensional amplifier model can be correctly applied. Fig. 5 reports on VSL measurements performed on sample 5A (39 at% Si). If one applies Eq. (1) in the length range where the pump is not constant, as in Fig. 5b, an artificial positive gain coefficient of  $84 \text{ cm}^{-1}$  can be erroneously deduced. As demonstrated in Fig. 5a with the measurement of the scattered pump laser intensity, it is clear that the

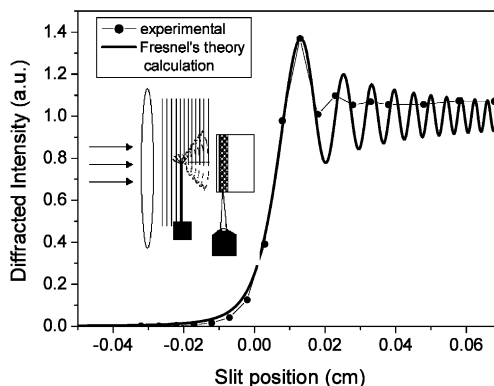


Fig. 4. Fresnel diffraction of the pump laser beam by the variable slit: experimental data (points) and calculation (solid line). Inset: sketch of the straight-edge diffraction of the pump laser from the variable slit.

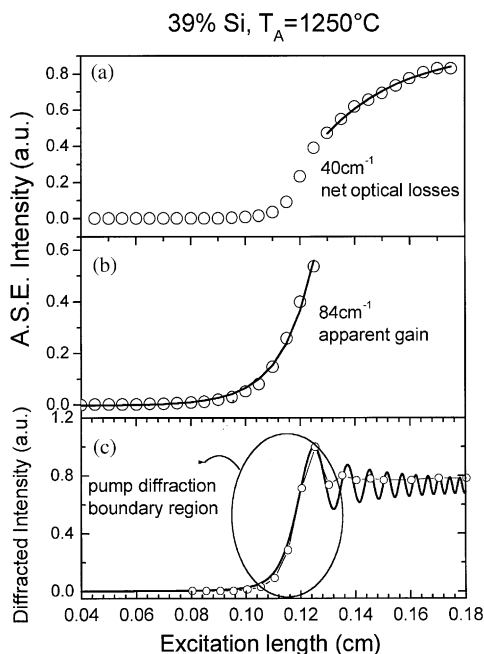


Fig. 5. Room temperature VSL measurement for sample 5A (39 at% Si). (a) Fit of the data of the linear excitation regime (solid line) yields optical losses of  $40 \text{ cm}^{-1}$ . (b) Fit of the data in the pump diffraction range with the VSL model yields an apparent gain of  $84 \text{ cm}^{-1}$ . (c) Pump laser beam diffraction profile measured (points) and calculation (solid line).

length region where it makes sense to start the fitting corresponds to the range where the diffraction of the laser yields constant pump intensity on the sample. In

Fig. 5a, the VSL data are fitted for excitation lengths where the pump intensity is constant and approximately equal to 3 kW/cm<sup>2</sup>, yielding optical losses of 40 cm<sup>-1</sup>. Without a careful pump diffraction analysis the proper range for VSL data interpretation and fitting would have remained uncertain.

#### 4. Continuous wavelength (CW) excitation VSL results

We have performed CW excitation VSL measurements by using an UV extended Argon laser ( $\lambda_{exc} = 365$  nm, maximum power 600 mW). The laser beam has been focused through a cylindrical lens on a straight line about 10  $\mu$ m wide and 1.5 mm long. A movable slit has been used to vary the length of the excited sample region which coincided with the waist of the Gaussian laser beam [27]. This yields a reduced accessible length range of roughly 0.8 mm. The amplified spontaneous emission spectra have been collected through a double monochromator and detected by a photomultiplier operating in photon counting mode.

Fig. 6 shows different VSL curves obtained on sample 3A (42 at% Si) at different detection wavelengths ranging from 840 to 760 nm and at three different pumping intensities. The maximum measured peak net modal gain was  $g = 52 \pm 5$  cm<sup>-1</sup> at 760 nm for 3 kW/cm<sup>2</sup> (see Fig. 6b). Note that the peak gain wavelength is blue-shifted by 100 nm with respect to the luminescence peak wavelength (Table 1). The modal gain spectrum for this sample is wide and flat: an appreciable gain coefficient of 30 cm<sup>-1</sup> has been measured at 860 nm, too. The excitation intensity dependence of the modal gain is shown in Fig. 7. A transparency threshold of 0.5 kW/cm<sup>2</sup> can be extracted. From Eq. (1), the modal gain spectrum can be evaluated by using

$$g = \frac{1}{l} \left[ \ln \left( \frac{I_{ASE}(2l)}{I_{ASE}(l)} - 1 \right) \right]. \quad (3)$$

Fig. 8 compares the modal gain spectrum of sample 1A (46 at% Si) with the luminescence spectrum of the same sample. Modal gain values as high as 60 cm<sup>-1</sup> have been measured at 730 nm for an excitation intensity of 3 kW/cm<sup>2</sup>. A blue-shift of the gain with respect to the luminescence is also here observed.

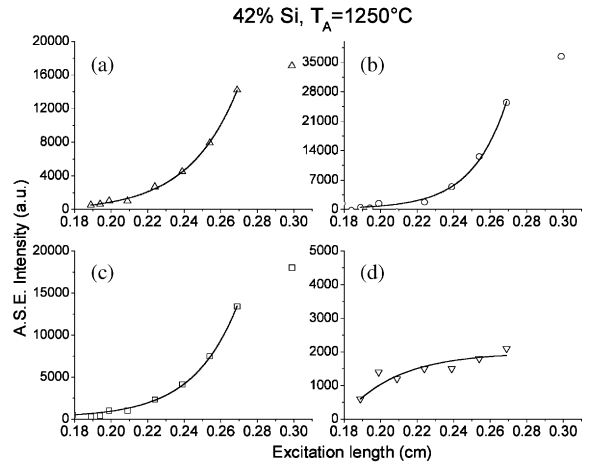


Fig. 6. Room temperature VSL curves on Si-nc sample 3A (42 at% Si). The symbols are the data while the lines are the fit with Eq. (1). (a) VSL at 840 nm at a pumping intensities of 1 kW/cm<sup>2</sup>. The fit yields a net modal gain coefficient of  $37 \pm 5$  cm<sup>-1</sup>. (b) VSL at 760 nm at a pumping intensity of 3 kW/cm<sup>2</sup>. The net modal gain coefficient is  $52 \pm 5$  cm<sup>-1</sup>. (c) VSL at 760 nm at a pumping intensities of 1 kW/cm<sup>2</sup>. The net modal gain is  $41 \pm 3$  cm<sup>-1</sup>. (d) Low power VSL curve at 760 nm (0.05 kW/cm<sup>2</sup>). The fit yields optical losses of  $34 \pm 5$  cm<sup>-1</sup>.

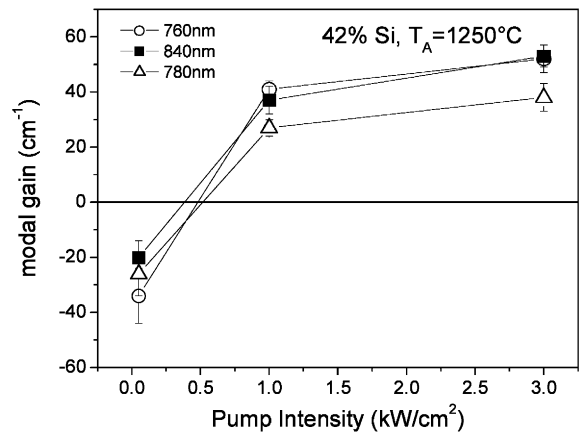


Fig. 7. Pump intensity dependence of the modal gain coefficient at three different detection wavelengths. This results are obtained on sample 3A (42 at% Si).

The modal gain line width is 120 nm while the luminescence line width is 215 nm.

Table 1 summarizes the VSL measurements on the three samples. The optical gain is given as the nano-crystal gain cross-section,  $\sigma_g$ , which is determined

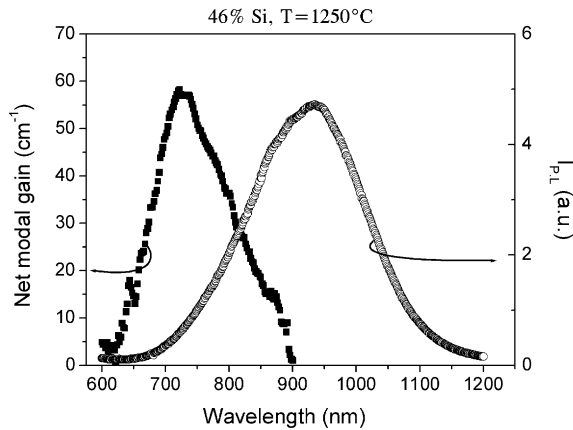


Fig. 8. Modal gain spectrum (filled squares) and luminescence spectrum (empty circles) for Si-nc sample 1A (46 at% Si).

from the net modal gain by using

$$\sigma_g = \frac{g}{\Gamma\rho}, \quad (4)$$

where  $\rho$  is the Si-nc density and  $\Gamma$  the optical confinement factor. Different wavelengths show different  $\sigma_g$ . Note that VSL measurements are sensitive only to the net modal gain of the material, namely the difference between the material gain and the waveguide

propagation losses. Since propagation losses can vary from one sample to the other it is not always possible to measure VSL modal gain even if the Si-nc population is inverted. We think that this is the case of sample 5A (39 at% Si). For the other samples we significantly measured gain in a spectral region blue-shifted with respect to the luminescence. This suggests that the active (amplifying) Si-nc can be just a fraction of the entire Si-nc distributions and that a strong competition among the different Si-nc occurs.

## 5. Time-resolved results

To investigate the stimulated emission dynamics time-resolved experiments are performed in two different configurations. When luminescence is measured in a  $45^\circ$  configuration, stimulated emission lifetimes are measured. This approach is less sensitive than VSL to the waveguide propagation losses as no optical mode propagates through the sample. When the VSL configuration is used (TR-VSL), the stimulated emission build-up time is measured as the signal photon flux propagates along the amplification axis. We used high fluencies short optical pulses (6 ns, 10 Hz, 430 nm) produced by an optical parametric oscillator pumped

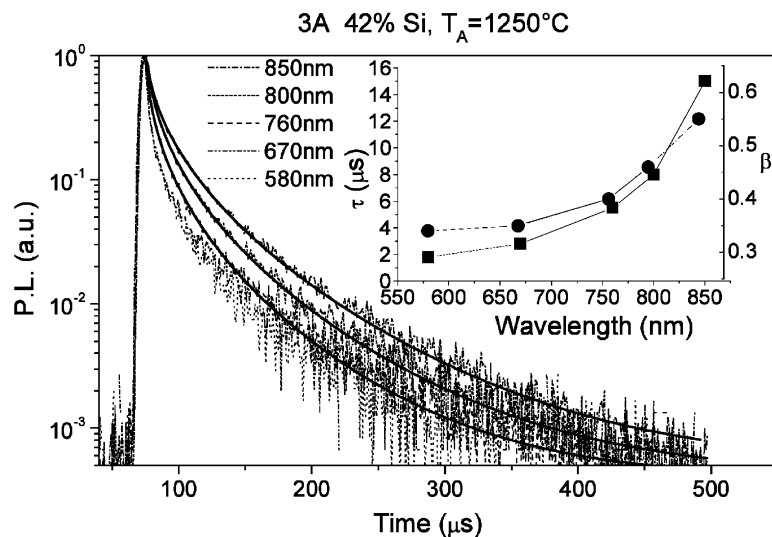


Fig. 9. Luminescence decays at the specified observation wavelengths. The thick lines are stretched exponential fits,  $I(t)=I(0)\exp(-(t/\tau)^\beta)$ , of the experimental data. The inset shows the stretched exponential  $\beta$  factor (circles) and the effective lifetime  $\tau$  (squares) as a function of the observation wavelength. The excitation intensity was  $0.5 \text{ mJ/cm}^2$ .

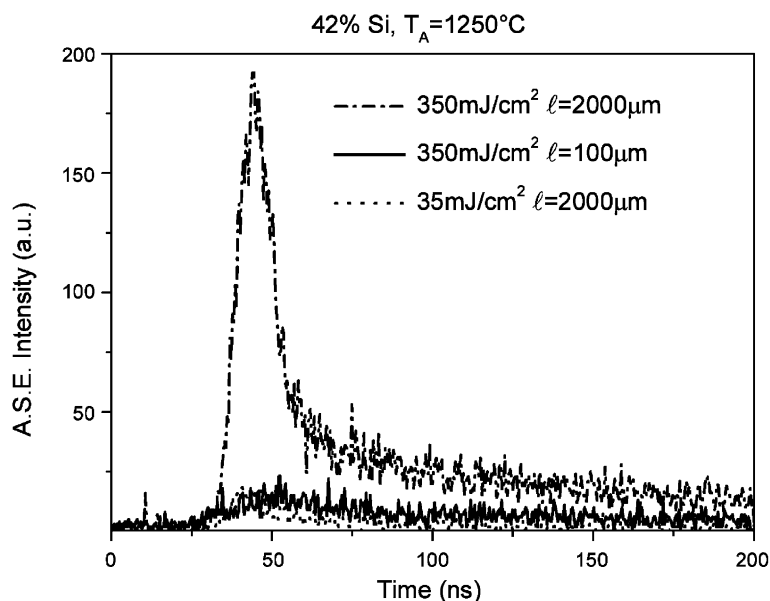


Fig. 10. High fluence time-resolved VSL on sample 3A (42 at% Si). The observation wavelength was 750 nm and the detection time window was 200 ns.

by the third harmonic of a Nd-YAG pulsed laser to excite the samples. We detect the radiation through a single grating spectrometer and a Hamamatsu Streak camera with ps resolution.

Fig. 9 shows the luminescence decays at low fluence ( $J_p$ ) obtained on sample 3A (42 at% Si). The decays are stretched exponentially with observation energy dependent lifetimes in the range of several  $\mu$ s, as already reported [28].

The most striking experimental findings appear when we perform high  $J_p$  measurements in VSL configuration. When  $\ell$  increases from 100 to 2000  $\mu$ m at a fixed  $J_p$ , Fig. 10 shows the appearance of a 15 ns long fast contribution overlapped to the usual slow component in the Si-nc luminescence decay. Fig. 10 shows also that the fast contribution disappears when, at fixed  $\ell$  of 2000  $\mu$ m,  $J_p$  is decreased and when, at fixed  $J_p$  of 350 mJ/cm<sup>2</sup>,  $\ell$  is reduced. These last observations allow us to rule out the Auger as the origin of the fast component, since the  $J_p$  intensity does not depend on  $\ell$ , while the Auger rate depends critically on the  $J_p$  intensity. The spectral dependence of the fast and slow component (see Fig. 11) demonstrates a strong blue-shift of the Si-nc light emission in the early nanoseconds after the pulse excitation. A com-

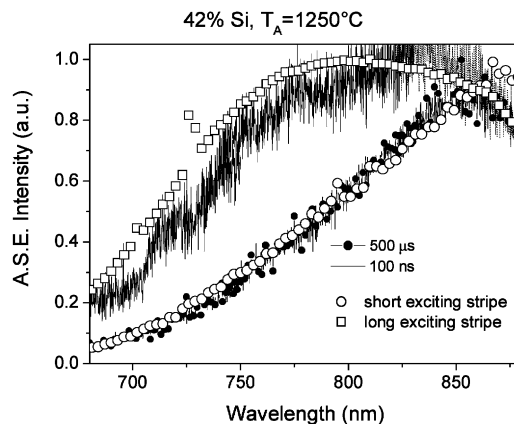


Fig. 11. Line shape of the time-resolved amplified spontaneous emission measured in VSL and integrated for a time interval of 500  $\mu$ s or 100 ns after the arrival of the exciting pulse. Empty symbols refer to the amplified spontaneous emission line shape for an excitation length of 100  $\mu$ m (named short, circles) or 600  $\mu$ m (named long, squares) measured in the CW VSL experiment for the 3A (42 at% Si) sample.

parison with the CW VSL measurements, reported in Fig. 11, shows that the fast component has a spectral shape similar to the ASE band measured for long  $\ell$

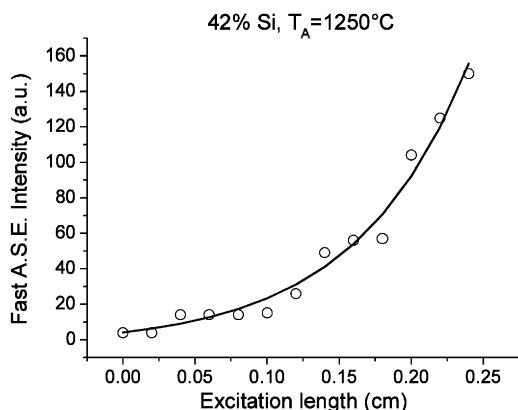


Fig. 12. Room temperature time-resolved VSL curve on sample 3A (42 at% Si). The fast peak intensity is plotted versus the excitation length on the sample. The excitation wavelength was 430 nm at a fluence of  $200 \text{ mJ/cm}^2$ . The detection wavelength was 840 nm and the gain coefficient deduced from the fit is  $12 \text{ cm}^{-1}$ .

(where strong amplification is expected), while the slow component spectrally overlaps the luminescence measured for short  $\ell$  (where negligible amplification occurs). To our opinion these are clear evidences of the fast stimulated emission lifetime in Si-nc.

Fig. 12 shows the result of a TRVSL measurement performed on sample 3A (42 at% Si). The fit of the peak emission vs.  $\ell$  data with Eq. (1) yields net modal gain coefficients ranging from  $8 \pm 3$  to  $20 \pm 2 \text{ cm}^{-1}$  depending on the detection wavelength. Lower values than those reported in the previous section are measured due to the longer wavelength of the pump laser. As expected for the stimulated emission rate, the fast component becomes faster as  $\ell$  increases (Fig. 13) because of the increased photon flux. As a further confirmation of the nature of the fast component, we show its intensity threshold behaviour as a function of  $J_p$  (see Fig. 14). On the contrary, sample 5A (39 at% Si), where no optical gain has been measured, shows a linear power curve characteristic.

## 6. Rate equation model

Although a full theoretical model of the stimulated emission processes in Si-nc is still lacking, a rather simplified phenomenological approach is possible. On the basis of the experimental findings we propose

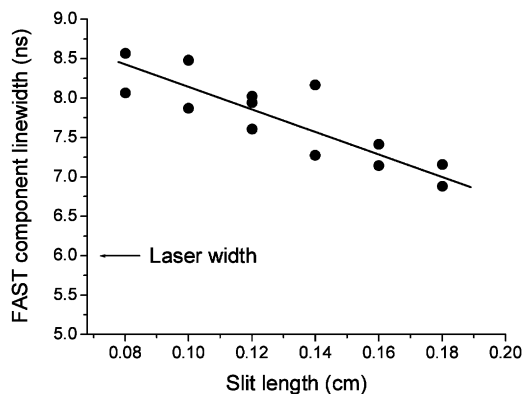


Fig. 13. Full-width at half-maximum of the fast component of the ASE decay measured for various excitation lengths on sample 3A (42 at% Si). The scatter of the points gives an indication of the errors in the measurements. The excitation fluence was  $110 \text{ mJ/cm}^2$ . The full-width at half-maximum of the pump laser is 6 ns.

a rate equation model to explain the major features of our experiments: (i) the almost complete absence of optical absorption at the peak gain emission for all the amplifying Si-nc samples, Fig. 2; (ii) a moderate low pumping threshold of about  $0.5 \text{ kW/cm}^2$  for population inversion, Fig. 7(iii) time-resolved VSL are characterized by a fast recombination component with a power threshold behaviour, which depends on the excitation slit length. We must specify that fast recombination dynamics in the range of some ns are typical of Auger non-radiative processes in p-Si [29,30]. The fast dynamics of its own is not enough to claim for optical amplification. A strong competition between Auger fast processes and stimulated emission is present in Si-nc. For some sample, Auger can prevail. As an example, sample 5A shows a fast recombination dynamics in the ns range, but unlike the amplifying samples 1A and 3A, no exponential VSL line shape, nor intensity threshold, have been measured. On the contrary, negative gain of the order of  $-5 \text{ cm}^{-1}$  has been found at the maximum pumping fluence. Sample 5A is indeed characterized by a low refractive index, as reported in Table 1, therefore a low modal confinement is expected in this case, yielding too high optical losses which overcome the modal gain.

Items (i) and (ii) can be explained within an effective four-level model reported on Fig. 15 (energy

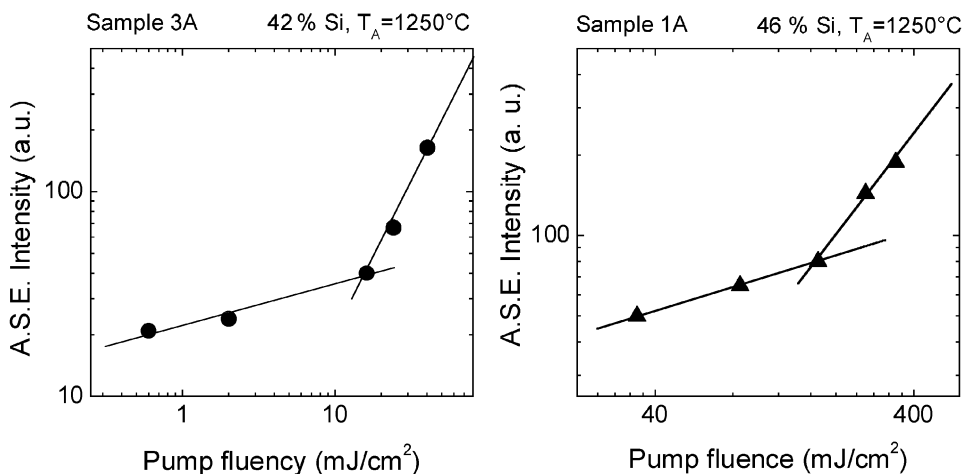


Fig. 14. Amplified spontaneous emission intensity as a function of the pump fluency for sample 3A (42 at% Si) (left) and sample 1A (46 at% Si) (right), excited in a VSL geometry at a fixed excitation length of 2 mm. The observation wavelength was 750 nm.

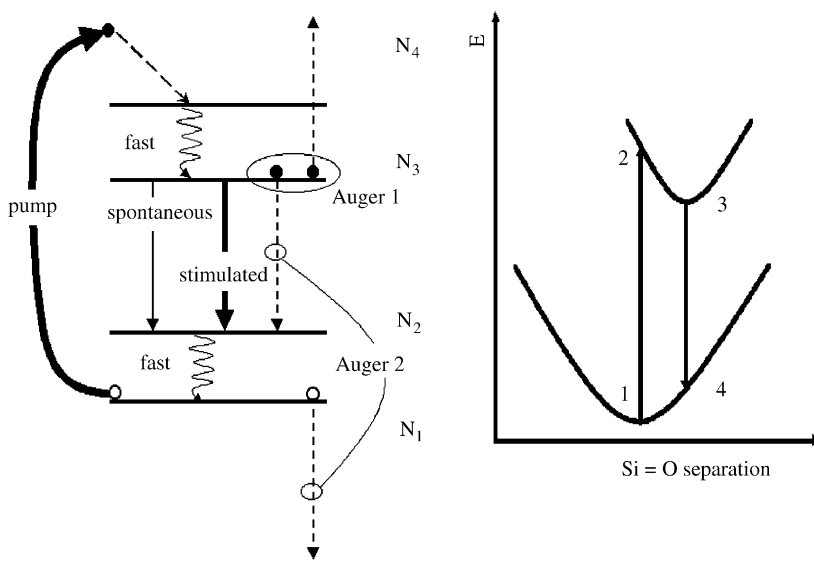


Fig. 15. (Left) Four-level system that has been introduced to model qualitatively the recombination dynamics under gain conditions. (Right) Schematic of the energy-configuration diagram of the silicon nanocrystals in an oxygen rich matrix. Radiative states are formed inside the nanocrystal band gap by the interface oxygen atoms. The excited nanocrystal state can occur at a different lattice coordinate with respect to the ground state.

levels scheme). The corresponding set of rate equations for photons and carriers includes both amplified spontaneous emission and Auger recombination. In particular, we assume that levels 2–4 are empty before the excitation occurs. Once the pumping starts,

levels begin to be populated and two different Auger non-radiative recombination processes can in principle take place. The first mechanism consists in an electron relaxation from energy level 3 to level 2 with the energy given to a second electron which is also

present in the same level 3 and which is promoted to higher lying levels in the conduction band, from which a very fast relaxation to level 4 occurs. This Auger process involves two electrons in the same level, and therefore the rate of such a process depends quadratically through a coefficient  $C_{A1}$  on the level population  $N_3$ . Another Auger mechanism involving an electron in the third level and a free hole in the valence band edge (level 1) can in principle occur, where the hole is sent deep in the valence band and then very rapidly relaxes again to the band edge. This process, has to be proportional, through a coefficient  $C_{A2}$ , to the product of the population of the emitting level 3 ( $N_3$ ) and the hole concentration in the valence band edge ( $N_h$ ).  $N_h$  equals the total concentration of electrons in the various excited levels, that is  $N_h = N_2 + N_3 + N_4$ . Within the four-level scheme we are proposing, the relaxation times of electrons from levels 4 and 2 are so fast that  $N_4$  and  $N_2$  are always almost empty. Therefore  $N_h \approx N_3$ . Hence, the following set of coupled rate equation has to be integrated:

$$\begin{aligned} \frac{dN_1}{dt} &= -\sigma_P \phi_P(t) N_1 + \Gamma_{21} N_2, \\ \frac{dN_2}{dt} &= \frac{N_3}{\tau} - \Gamma_{21} N_2 + B n_{\text{ph}} (N_3 - N_2) \\ &\quad + (C_{A1} + C_{A2}) N_3^2, \\ \frac{dN_3}{dt} &= -\frac{N_3}{\tau} - B n_{\text{ph}} (N_3 - N_2) + \Gamma_{43} N_4 - C_A N_3^2, \\ \frac{dN_4}{dt} &= C_{A1} N_3^2 + \sigma_P \phi_P(t) N_1 - \Gamma_{43} N_4, \\ \frac{dn_{\text{ph}}}{dt} &= V_a B n_{\text{ph}} (N_3 - N_2) - \frac{n_{\text{ph}}}{\tau_{\text{ph}}} + \beta \frac{N_3}{\tau_R}, \end{aligned} \quad (5)$$

where  $N_i$  represent the level population densities ( $i = 1, \dots, 4$ ),  $\sigma_P$  is the absorption cross-section at the wavelength of the pump,  $\phi_P$  is the time-dependent pumping photon flux,  $\Gamma_{ij}$  are the relaxation rates from the  $i$  to the  $j$  energy levels,  $\tau$  is the total lifetime of the emitting level  $N_3$ ,  $B$  is the stimulated transition rate which implicitly contains the gain cross-section  $\sigma$ ,  $n_{\text{ph}}$  is the emitted photons number,  $V_a$  is the optical mode volume,  $\tau_{\text{ph}}$  is the photon lifetime,  $\beta$  is the spontaneous emission factor and  $\tau_R$  is the radiative lifetime of  $N_3$ .  $C_A$  is an effective Auger coefficient

equal to  $2C_{A1} + C_{A2}$ , taking into account both of the two particles Auger processes (e–e or e–h).

It is possible to observe optical gain whenever the stimulated emission rate is greater than the Auger recombination rate. From Eq. (5) it is possible to define a stimulated emission lifetime as

$$\tau_{\text{se}} = \frac{1}{B n_{\text{ph}}} = \frac{4}{3} \pi R_{\text{nc}}^3 \frac{1}{\xi \sigma c n_{\text{ph}}}, \quad (6)$$

where we have introduced the Si-nc volume fraction  $\xi$  and where the relation,  $B = \sigma c / V$ , valid under the assumption of monochromatic incident light, is used. It is worth noticing that the inverse dependence of  $\tau_{\text{se}}$  on  $\xi$  and on  $\sigma$ , as discussed in Ref. [31]. An equivalent Auger recombination time can be defined as follows:

$$\tau_A = \frac{1}{2C_A N_3}. \quad (7)$$

It is clear from the discussion that to observe optical gain  $1/\tau_{\text{se}} \geq 1/\tau_A$ ; or equivalently, if we define a competition factor  $C = \tau_A/\tau_{\text{se}}$ ,  $C \geq 1$ . This poses a condition on the volume fraction.

The proposed rate equation model fits qualitatively the experimental data. Fig. 16 shows an example. It turned out that gain cross section of the order of  $10^{-17}$  cm<sup>2</sup> are large enough to compensate for Auger processes as fast as 1 ns in our best samples. Competition factors as high as 1.1–1.5 (depending both on the sample characteristics and excitation rates) can be deduced by these decay line shape analysis.

## 7. Discussion

The observation of optical gain in both ion implanted [12] and PECVD formed Si-nc demonstrates that this effect is not exclusively related to the Si-nc preparation processes but it is an intrinsic property of the Si-nc themselves. Unfortunately, the key material parameters that determine the possibility of having optical gain are not yet fully mastered. Despite of a clear understanding of the gain mechanism is still lacking, the field is under rapid improvement and other groups reported results similar to ours [13–15].

Here, we have proposed an effective four-level model to treat qualitatively the strong competition between Auger recombination and stimulated emission.

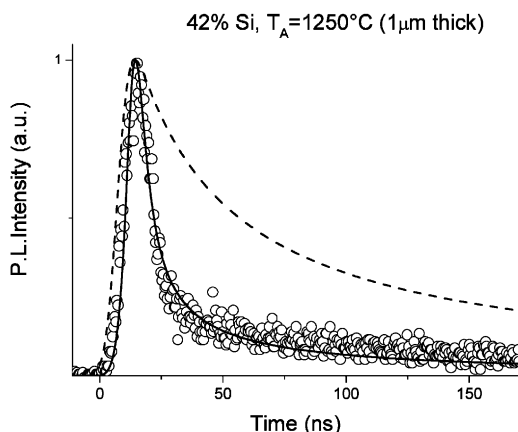


Fig. 16. (Symbols) Room temperature time-resolved decay curve on a sample with the same production parameters as sample 3A (42 at% Si) but a larger thickness of 1  $\mu\text{m}$ . The detection wavelength was 750 nm. (Solid line) Emitted photon numbers obtained by solving the four levels model with an Auger lifetime of 20 ns, a gain cross-section of  $1.2 \times 10^{-17} \text{ cm}^2$ , a Si-nc density of  $6 \times 10^{18} \text{ cm}^{-3}$  and a pumping photon flux of  $10^{19} \text{ photons}/(\text{s cm}^2)$ . (Dashed line) Emitted photon numbers obtained by solving the four levels model with the same parameters but neglecting stimulated emission. All the curves are normalized to unity.

This is still a phenomenological model and we need a theory of the optical properties of Si-nc in  $\text{SiO}_2$  and of their interface. However, we can suggest a possible nature for this four-level model. From X-ray absorption studies and *ab initio* calculations [32], strong evidences emerge that the Si-nc are coated by a 1 nm thick transition region that constitutes a shell of stressed silica on Si-nc. One can speculate that this stressed  $\text{SiO}_2$  layer enhances the formation of interface oxygen-related states (silanone?) on the surface of Si-nc, which can relax when excited. A sketch of such energy-configuration diagram is shown in Fig. 15. Many theoretical papers [18–20], reports the energetic of silanone-like molecule as a function of the Si=O interatomic distances. Fig. 15 shows that when electrons/holes are excited, they can relax into the Si=O surface states which in turn undergo a lattice relaxation modifying their energetic. Within this scheme the 1 and 4 levels of the rate equations are associated with pure Si-nc states while the 2 and 3 levels to the ground and excited silanone states.

## 8. Conclusions

Gain has been measured on a set of PECVD Si-nc samples produced by high temperature annealing at  $1250^\circ\text{C}$  of  $\text{SiO}_x$  thin films with different silicon contents. Continuous-wave UV excitation VSL measurements show a low threshold ( $0.5 \text{ kW}/\text{cm}^2$ ) positive optical gain of the order of  $50 \text{ cm}^{-1}$  at pumping intensities of  $3 \text{ kW}/\text{cm}^2$ . Large Stokes-shift between luminescence and gain has been found. High power time-resolved luminescence and VSL have been performed showing the onset of stimulated emission. Superlinear light emission and stimulated emission lifetime narrowing have been demonstrated. A four-level model which includes amplified spontaneous emission and Auger processes has been introduced and a simple criterion for the onset of optical gain in Si-nc samples has been proposed. Good qualitative agreement with measured time-resolved decays has been found.

## Acknowledgements

This work has been supported by the National Institute for the Physics of Matter (INFN) through the advanced research project RAMSES. We acknowledge fruitful discussion with S. Ossicini and his theoretical group.

## References

- [1] W.P. Dumke, Phys. Rev. 127 (1962) 1559.
- [2] L.T. Canham, Appl. Phys. Lett. 57 (1990) 1046.
- [3] K.D. Hirschman, L. Tsybeskov, S.P. Dutttagupta, P.M. Fauchet, Nature 384 (1996) 338.
- [4] P.M. Fauchet, J. Lumin. 80 (1999) 53.
- [5] Y. Kanemitsu, T. Ogawa, K. Shiraishi, K. Takeda, Phys. Rev. B 48 (1993) 4883.
- [6] T. Shimizu-Iwayama, K. Fujita, S. Nakao, K. Saitoh, T. Fujita, N. Itoh, J. Appl. Phys. 75 (1994) 7779.
- [7] L.N. Dinh, L.L. Chase, M. Balooch, L. Terminello, F. Wooten, Appl. Phys. Lett. 65 (1994) 3111.
- [8] T. Inokuma, Y. Wakayama, T. Muramoto, R. Aoki, Y. Kurata, S. Hasegawa, J. Appl. Phys. 83 (1998) 2228.
- [9] Z.H. Lu, D.J. Lockwood, J.M. Baribeau, Nature 378 (1995) 258.
- [10] D.J. Lockwood, Z.H. Lu, J.M. Baribeau, Phys. Rev. Lett. 96 (1996) 539.

- [11] L. Pavesi, E. Buzaneva (Eds.), *Frontiers of Nano-Optoelectronic Systems*, NATO Science Series, Kluwer Academic Publishers, Dordrecht, 2000.
- [12] L. Pavesi, L. Dal Negro, C. Mazzoleni, G. Franzò, F. Priolo, *Nature* 408 (2000) 440.
- [13] L. Khriachtchev, M. Rasanen, S. Novikov, J. Sinkkonen, *Appl. Phys. Lett.* 79 (2001) 1249.
- [14] M. Nayfeh, S. Rao, N. Barry, J. Therrien, G. Belomoin, A. Smith, S. Chaieb, *Appl. Phys. Lett.* 80 (2002) 121.
- [15] K. Luterova, I. Pelant, I. Mikulskas, R. Tomasiunaset, D. Muller, J.-J. Grob, J.-L. Rehspringer, B. Honerlage, *J. Appl. Phys.* 91 (2002) 2896.
- [16] M.V. Wolkin, J. Jorne, P.M. Fauchet, G. Allan, C. Delerue, *Phys. Rev. Lett.* 82 (1999) 197.
- [17] F. Iacona, G. Franzò, C. Spinella, *J. Appl. Phys.* 87 (2000) 1295.
- [18] R.J. Baierle, M.J. Caldas, E. Molinari, S. Ossicini, *Solid State Commun.* 102 (1997) 545.
- [19] F. Zhou, J.D. Head, *J. Phys. Chem. B* 104 (2000) 9981.
- [20] A.B. Filonov, S. Ossicini, F. Bassani, F. Arnaud d'Avitaya, *Phys. Rev. B* 65 (2002) 195317.
- [21] A. Puzder, A.J. Williamson, J.C. Grossman, G. Galli, *Phys. Rev. Lett.* 88 (2002) 97401.
- [22] V.I. Klimov, Ch.J. Schwarz, D.W. McBranch, C.W. White, *Appl. Phys. Lett.* 73 (1998) 2603.
- [23] A. Yu Kobitski, K.S. Zhuravlev, H.P. Wagner, D.R.T. Zahn, *Phys. Rev. B.* 63 (2001) 115423.
- [24] K.L. Shaklee, R.E. Nahaori, L.F. Leheny, *J. Lumin.* 7 (1973) 284.
- [25] P.W. Milonni, J.H. Eberly, *Lasers*, Wiley, New York, 1988.
- [26] A. Sommerfeld, *Optics*, Academic Press, London, 1967.
- [27] L. Pavesi, L. Dal Negro, M. Cazzanelli, et al., *Proc. SPIE* 4293 (2001) 162.
- [28] J. Linnros, A. Galeckas, N. Lalic, V. Grivickas, *Thin Solid Films* 297 (1997) 167.
- [29] C. Delerue, M. Lanoo, G. Allan, E. Martin, I. Mihalcescu, J.C. Vial, R. Romenstain, F. Muller, A. Bsiesty, *Phys. Rev. Lett.* 75 (1995) 2228.
- [30] R. M'ghaieth, H. Maaref, I. Mihalcescu, J.C. Vial, *Phys. Rev. B.* 60 (1999) 4450.
- [31] V. Klimov, A. Mihkailovsky, A. Malko, J. Hollingsworth, C. Leatherdale, M. Bawendi, *Science* 290 (2000) 314.
- [32] N. Daldosso, M. Luppi, S. Ossicini, E. Degoli, R. Magri, G. Dalba, P. Fornasini, R. Grisenti, F. Rocca, L. Pavesi, F. Priolo, F. Iacona, *Phys. Rev. Lett.*, submitted for publication.